ORIGINAL PAPER

CrossMark

Spatio-temporal Reconstruction of Neural Sources Using Indirect Dominant Mode Rejection

Alireza Talesh Jafadideh[1] · Babak Mohammadzadeh Asl[1]

Abstract
Adaptive minimum variance based beamformers (MVB) have been successfully applied to magnetoencephalogram (MEG) and electroencephalogram (EEG) data to localize brain activities. However, the performance of these beamformers falls down in situations where correlated or interference sources exist. To overcome this problem, we propose indirect dominant mode rejection (iDMR) beamformer application in brain source localization. This method by modifying measurement covariance matrix makes MVB applicable in source localization in the presence of correlated and interference sources. Numerical results on both EEG and MEG data demonstrate that presented approach accurately reconstructs time courses of active sources and localizes those sources with high spatial resolution. In addition, the results of real AEF data show the good performance of iDMR in empirical situations. Hence, iDMR can be reliably used for brain source localization especially when there are correlated and interference sources.

Keywords Brain source localization · Electroencephalography (EEG) · Indirect dominant mode rejection (iDMR) · Magnetoencephalography (MEG) · Minimum variance beamformer (MVB)

Introduction

Synchronous activations of tens of thousands neurons within the brain could generate magnetic field and electrical potential outside of the head that can be registered by an array of sensors of magnetoencephalography (MEG) and electroencephalography (EEG), respectively. This population of neurons, in most cases, can be modeled by an electrical dipole, also called a source, having parameters including position, orientation, and amplitude.

Estimating the output of sensors positioned near or on the scalp for a given electrical dipole parameters involves well-conditioned forward problem, the solution of which yields to the lead field matrix or also named gain matrix. Estimating the brain source parameters from measured data and consequently mapping brain activity at the source level requires solving a so-called inverse problem. In contrast to

the forward problem, the inverse problem is ill-posed (Baillet et al. 2001; Greenblatt et al. 2005), since the number of candidates for source location in the brain (voxel) is much larger than the number of recording sensors, therefore many source distributions can be inferred for one measurement.

Various kinds of methodologies have been presented for solving the salient inverse problem such as minimum $\ell2$-norm estimation (MNE) (Baillet et al. 2001; Dinh et al. 2015; Dai et al. 2012), multiple signal classification (music) (Mosher and Leahy 1992, 1998, 1999; Shahbazi et al. 2015), minimum current estimation (MCE) (Uutela et al. 1999), minimum variance beamforming (MVB) (Greenblatt et al. 2005; Sekihara and Nagarajan 2008; Veen et al. 1997; Huang et al. 2004; Jonmohamadi et al. 2014; Moiseev and Herdman 2013; Haufe and Arne 2016; Mills et al. 2012), FOCUSS (Gorodnitsky et al. 1995), sLORETA (Pascual-Marqui 2002; Chowdhury et al. 2015). Recursively applied and projected (RAP)-MUSIC is a subspace signal processing approach attempting to find the source locations by using a recursive procedure (Mosher and Leahy 1998). Although RAP-MUSIC shows good performance in source localizing even in the presence of highly correlated sources (Xu et al. 2004), it cannot reconstruct time course of sources. Also, because of the mentioned drawback, Rap-MUSIC is not

---

✉ Babak Mohammadzadeh Asl
   babakmsl@modares.ac.ir

[1] Department of Electrical and Computer Engineering, Tarbiat Modares University, Tehran, Iran

able to map brain activity in every millisecond and has the temporal resolution in the order of a few hundred milliseconds (time of data that is used for computing measurement covariance matrix).

MVB is an adaptive spatial filter type method whose filter should reveal time course for a given location and eliminate activities originated from other locations. The temporal resolution is of the order of millisecond and makes MVB suitable for applications dealing with time course. A variant of MVB is regularized MVB (RMVB) (Brookes et al. 2008; Tikhonov and Arsenin 1997) in which the data covariance matrix is diagonally loaded to ensure a statistically stable covariance matrix, to improve the robustness and to increase the output SNR. However, all these advantages come at the expense of a decreased spatial resolution. In publication by Sekihara et al. (2001), vector version of Borgiotti–Kaplan beamformer was developed and the derived spatial filter was projected onto the signal subspace. By doing so, the resulting beamformer produced higher output SNR as well as higher spatial resolution compared with the MVB. The performance of MVB, RMVB, and eigenspace-projection Borgiotti–Kaplan beamformer is deteriorated particularly in reconstructing time courses of sources at situations where highly correlated and interference sources exist.

Many algorithms have been developed in recent decade to solve this problem (Kimura et al. 2007; Brookes et al. 2007; Dalal et al. 2006; Popescu et al. 2008; Quraan and Cheyne 2010; Hui et al. 2010). Kimura et al., at first step, estimated the brain activity covariance matrix by the minimum norm method, then sources were "decorrelated" by discarding the non-diagonal terms of that matrix. Finally, a new version of the measurement covariance matrix was generated and used in the beamformer analysis.

Popescu et al. used only sensors that were close enough to one of the correlated sources, or to use just one hemisphere of the sensor array. By doing so, the contribution to the covariance from another source is greatly reduced. This is achieved at the cost of decreasing the signal to noise ratio (SNR) and the spatial resolution for non-coherent activations. This technique is used for bilateral activations and so needs a priori knowledge for a suitable performance.

In the approach taken by Brookes et al. (2007), the source correlations are incorporated into the lead field matrix. The new lead field matrix is composed as a linear combination of the dipolar forward solutions of participating sources. The most significant problem here is that the reconstructed time course is a linear combination of the time courses of the participating sources.

In publications by both Dalal et al. (2006) and by Hui et al. (2010), additional constraints are imposed on the beamformer weights so that the beamformer gain from certain brain regions are (approximately) zero. Without a priori knowledge of the locations of likely interfering sources, this

region is large and the decrease in SNR and spatial resolution may become significant.

In this paper, an approach for reconstructing spatio-temporal source activity is proposed when highly correlated and interference sources exist. This method, which previously has been employed in wireless communications (Santos et al. 2007), can accurately reconstruct time courses of sources in both aspects of shape and amplitude, and thereby provide high spatial and temporal resolution and output SNR. New technique is indirect dominant mode rejection (iDMR). For implementing iDMR, at first, source locations and orientations are respectively found by RAP-MUSIC and by solving an eigenvalue problem (Sekihara and Nagarajan 2008; Sekihara et al. 2004). RAP-MUSIC is exploited due to its capability in distinguishing the highly correlated sources. Then by using measurement and noise covariance matrices, lead field matrix and orientation vector of found sources, covariance matrix of sources is estimated. In the following, sources are "decorrelated" by discarding the non-diagonal terms of that matrix. New data covariance matrix is made based on the new covariance matrix of sources and replaced in MVB spatial filter. Finally, new spatial filter is employed for reconstructing spatio-temporal source activity.

The proposed scheme, as opposed to Popescu et al. uses all sensors thereby obtains suitable spatial resolution and output SNR. Unlike the proposed approach by Brookes et al., iDMR can easily find time course of each source. In works of Dalal et al. and of Hui et al., null constraints on some regions were applied which result in reduction of degrees of freedom, whereas zeroing off-diagonal elements of source covariance matrix is performed in iDMR which is a null constraint on interaction between sources not on gain matrix. Thus, iDMR preserves the degrees of freedom. Also, in this work, active source locations are found by RAP-MUSIC and hence, the problem of needing a priori knowledge regarding the location of interfering sources, in works of Dalal et al. and of Hui et al., is solved.

We compare iDMR approach with power-based multiple pseudo-z score localizer technique (MPZ) developed by Moiseev and Herdman (Moiseev et al. 2011) using simulated ERF data. This technique as with the iDMR employs a recursive search for finding active location. However, it uses a power based beamformer instead of RAP-MUSIC. Also, it attempts to find localized source time courses by applying a spatial filter which is designed to only pass activity of found sources and attenuate other undesired ones and noise.

EEG and MEG numerical experiments confirm that the proposed method outperforms the MVB, eigenspace-MVB and MPZ. The real AEF data results demonstrate the iDMR ability for empirical condition.

The rest of the paper is organized as follows. In the "Background" section data model is introduced, then MVB and power-based multiple source localizer (MPZ) for comparison

purpose and RAP-MUSIC because of using in iDMR are formulated. We formulate and describe the proposed method in section "Proposed Method". Experimental results using simulated EEG/MEG and real MEG data are presented at "Performance Evaluations" section, followed by "Discussion" section and a brief conclusion in "Conclusion" section.

Background

Data Model

With assuming linearity of the medium, post-stimulus observed data $\mathbf{x} \in \mathbb{R}^{M \times 1}$ by M sensors at time point $t \in \{1, 2, ..., K\}$ generated by L dipoles is modeled as

$$\mathbf{x}(t) = \sum_{l=1}^{L} \mathbf{H}(\mathbf{q}_l)\mathbf{m}_l s_l(t) + \mathbf{n}(t) \tag{1}$$

where $\mathbf{m}_l \in \mathbb{R}^{3 \times 1}$ is unit-norm vector indicating lth dipole orientation, $s_l(t)$ is time course of the lth dipole, $\mathbf{q}_l \in \mathbb{R}^{3 \times 1}$ is location of the lth dipole, $\mathbf{H}(\mathbf{q}_l) \in \mathbb{R}^{M \times 3}$ is gain matrix the first column of which is equal to the measured data when there is no noise and the dipole has unit magnitude in x direction and zero magnitude in y and z directions; similarly the second and third columns are for y and z directions, respectively, and $\mathbf{n}(t) \in \mathbb{R}^{M \times 1}$ represents noise vector. In this study, for simplicity we assume that each dipole has fixed orientation.

MVB Concept

One of the most popular beamformers is minimum variance beamformer that has widely been used in the sensor array signal processing especially reconstructing neural sources. The output of a MVB spatial filter (also called MVB weight matrix) for location $\mathbf{q}_0$ is

$$\mathbf{y}(t) = \mathbf{W}^T(q_0)\mathbf{x}(t) \tag{2}$$

where $\mathbf{W} \in \mathbb{R}^{M \times 3}$ is a column weight matrix and superscript "T" denotes the matrix transpose. The first column of ideal $\mathbf{W}$ assigns weights to $\mathbf{x}$ at time point t so that the weighted summation of measurements yields to the dipole activity in x direction at that time point; the second and third columns values are for revealing dipole activity in y and z directions, respectively. To this end, variance of the filter output $tr(\mathbf{R_y})$ which is due to the noise and activity of other sources is minimized while still by imposing a linear constraint activity at desired location is preserved. This idea can be formulated as

$$\min_{\mathbf{W}(\mathbf{q}_0)} tr(\mathbf{R_y}) = \min_{\mathbf{W}(\mathbf{q}_0)} tr[\mathbf{W}^T(\mathbf{q}_0)\mathbf{R}\mathbf{W}(\mathbf{q}_0)]$$
$$\text{subject to } \mathbf{W}^T(\mathbf{q}_0)\mathbf{H}(\mathbf{q}_0) = \mathbf{I}_3 \tag{3}$$

where $\mathbf{R} \in \mathbb{R}^{M \times M}$ is covariance matrix of observed data, $\mathbf{I}_3$ is 3-dimensional identity matrix, and $tr(.)$ denotes trace of matrix. When there are correlations between dipole activity in three directions x, y, z (this situation occurs in real data with high degree; in this paper because of using fixed orientation dipoles the correlation coefficient is 1), the source localization and time course estimation can be disrupted, so linear constraint used in MVB can perfectly eliminate this intra-dipole correlation. The solution of constrained optimization problem using Lagrange multiplier method is obtained as

$$\mathbf{W}_{MVB}(\mathbf{q}_0) = \mathbf{R}^{-1}\mathbf{H}(\mathbf{q}_0)(\mathbf{H}^T(\mathbf{q}_0)\mathbf{R}^{-1}\mathbf{H}(\mathbf{q}_0))^{-1}. \tag{4}$$

In practice, $\mathbf{R}$ is unknown and can be estimated by sample covariance matrix

$$\overline{\mathbf{R}} = \frac{1}{K} \sum_{t=1}^{K} \mathbf{x}(t)\mathbf{x}(t)^T. \tag{5}$$

The output power of spatial filter which is used for brain mapping is expressed as

$$P_{MVB}(\mathbf{q}_0) = tr(\mathbf{W}_{MVB}^T(\mathbf{q}_0)\overline{\mathbf{R}}\mathbf{W}_{MVB}(\mathbf{q}_0)). \tag{6}$$

Localizing data according to (6) results in too much misplacing, maxima of the power shifted toward to the center of the head. The reason for this inherent problem at beamformer based methods has been addressed in Van Veen et al. (1997) in which the adverse effect of presence of noise covariance matrix $\mathbf{Q}$ in the data covariance matrix $\mathbf{R}$ has been shown. To overcome this problem, we use single source power pseudo-Z value:

$$P_Z^{MVB}(\mathbf{q}_0) = \lambda_{\max}\{\mathbf{W}_{MVB}^T(\mathbf{q}_0)\overline{\mathbf{R}}\mathbf{W}_{MVB}(\mathbf{q}_0).$$
$$(\mathbf{W}_{MVB}^T(\mathbf{q}_0)\mathbf{Q}\mathbf{W}_{MVB}(\mathbf{q}_0))^{-1}\}. \tag{7}$$

where $\lambda_{\max}$ is the largest eigenvalue of the bracketed item and the time course of source positioned in $\mathbf{q}_0$ is given by

$$s_{MVB}(\mathbf{q}_0, t) = \mathbf{m}^T(\mathbf{q}_0)\mathbf{W}_{MVB}^T(\mathbf{q}_0)\mathbf{x}(t) \tag{8}$$

where $\mathbf{m}$ is dipole unit-norm vector orientation and can be found as

$$vec_{\min}\{\mathbf{W}_{MVB}^T(\mathbf{q}_0)\overline{\mathbf{R}}\mathbf{W}_{MVB}(\mathbf{q}_0).$$
$$(\mathbf{W}_{MVB}^T(\mathbf{q}_0)\mathbf{Q}\mathbf{W}_{MVB}(\mathbf{q}_0))^{-1}\} \tag{9}$$

where $vec_{\min}$ is the eigenvector associated to the smallest eigenvalue of the bracketed item.

Power-Based Multiple Source Localizer (MPZ)

In this subsection, we aim to formulate power-based multiple source localizer developed by Moiseev et al. (2011) which

somewhat is similar to the iDMR and has none of the disadvantages counted for (Brookes et al. 2007; Dalal et al. 2006; Popescu et al. 2008; Quraan and Cheyne 2010; Hui et al. 2010). Moiseev et al. derived several measures in which source location was determined by finding a global maximum of a localizer function defined on a parameter space of high dimension. To find global maxima for all sources, they developed an iterative algorithm. In this paper, we use MPZ localizer which is extended form of single pseudo-Z score and is employed for multiple sources localizing by a sequential procedure.

In a brief view, MPZ finds n sources by n times search over all the brain and in each time (or iteration) introduces location with maximum power as source location. In iteration k ($k < n$), spatial filter that is used for computing pseudo-Z score value for each location is orthogonal to the columns of the lead field matrix matrices of all the other sources found in previous $k-1$ iterations. In each iteration, localized source orientation is estimated using generalized eigenvalue problem. The locations of earlier found sources do not change but spatial filter is updated. Spatial filter at iteration k contains weights of all detected sources therefore by applying it to the data time courses of all k localized sources are obtained. Since weight of each iteration is orthogonal to the columns of the lead field matrix of the other iteration sources, one can probably obtain true time course without cancellation.

Mathematical details are presented now. The algorithm starts with a single source power pseudo-Z value. The largest activation detected is designated as first source. The orientation of found source is determined using (9). On step k of the algorithm we fix coordinates of previously found $(k-1)$ sources and label these as "references". The gain matrix $\mathbf{H}$ may be written as

$$\begin{aligned} \mathbf{H} &= \{\mathbf{H}^R, \mathbf{h}^k(\mathbf{r}^k)\}, \\ \mathbf{h}^k(\mathbf{r}^k) &= \mathbf{H}^k(\mathbf{r}^k)\mathbf{u}^k, \end{aligned} \tag{10}$$

where columns of a "reference" matrix $\mathbf{H}^R$ are forward solutions of already found sources and columns of matrix $\mathbf{H}^k$ are the gain vectors for sources at $\mathbf{r}^k$. To find source k, vector $\mathbf{r}^k$ is run over the entire brain and the largest eigenvalue λ of the following generalized eigenvalue problem is computed:

$$\mathbf{D}(\mathbf{r}^k)\mathbf{u}^k = \lambda \mathbf{F}(\mathbf{r}^k)\mathbf{u}^k, \tag{11}$$

where

$$\begin{aligned} \mathbf{D} &= \mathbf{A}^{kR}(\mathbf{A}^{RR})^{-1}\mathbf{B}^{RR}(\mathbf{A}^{RR})^{-1}\mathbf{A}^{Rk} - \\ &\quad \mathbf{A}^{kR}(\mathbf{A}^{RR})^{-1}\mathbf{B}^{RK} - \mathbf{B}^{kR}(\mathbf{A}^{RR})^{-1}\mathbf{A}^{Rk} + \mathbf{B}^{kk}, \\ \mathbf{F} &= \mathbf{A}^{kk} - \mathbf{A}^{kR}(\mathbf{A}^{RR})\mathbf{A}^{Rk}, \\ \mathbf{A} &= \mathbf{H}^T\overline{\mathbf{R}}^{-1}\mathbf{Q}\overline{\mathbf{R}}^{-1}\mathbf{H}, \\ \mathbf{B} &= \mathbf{H}^T\overline{\mathbf{R}}^{-1}\mathbf{H}. \end{aligned} \tag{12}$$

Here, $\mathbf{D}$ and $\mathbf{F}$ are 3×3 matrix. For first iteration, the $\lambda_{\max}$ of (11) is the same as (7). Location of source k is one $\mathbf{r}^k$ for which the maximum largest eigenvalue is derived. Then, $\mathbf{u}^k$ for found source is obtained as eigenvector corresponding to the largest eigenvalue of (11). The spatial filter in iteration k is attained by:

$$\mathbf{W}(\mathbf{r}^1, \ldots, \mathbf{r}^k) = \frac{\overline{\mathbf{R}}^{-1}\mathbf{H}}{\mathbf{H}^T\overline{\mathbf{R}}^{-1}\mathbf{H},}, \mathbf{W}^T\mathbf{H} = \mathbf{I}_k. \tag{13}$$

By passing data through $\mathbf{W}$, time courses of k found sources are reconstructed. For terminating the iteration, Moiseev et al. proposed monitoring single source power pseudo-Z values (7) of each new source. Iterations should be terminated when found source power becomes small and starts fluctuating around a baseline level.

RAP-MUSIC

The multiple signal classification (MUSIC) is a subspace scanning approach in which the lead field matrices of candidate locations throughout the brain are projected onto the signal subspace. Locations at which projection metric reaches to the local maxima are regarded as source locations. However, as stated by Mosher and Leahy, (Mosher and Leahy 1999) using the MUSIC often poses two problems. First, errors in estimating the signal subspace can make it difficult to differentiate "true" from "false" peaks in the MUSIC metric. Second, automatically finding several local maxima in the MUSIC metric becomes difficult as the dimension of the source space increases.

To overcome these problems, Mosher and Leahy introduce the idea of using a sequential procedure called recursively applied and projected (RAP)-MUSIC in which in each iteration one new source is found as global maximizer of cost function modified at that iteration. Modifying is carried out by projecting the gain matrix and signal subspace away from the subspace spanned by sources found in previous iterations.

At first iteration, location of first source yields to global maxima of

$$\overline{\boldsymbol{\theta}}_1 = \max_{\boldsymbol{\theta}}(\lambda_{\max}\{\mathbf{U}_1^T(\boldsymbol{\theta}_j)\mathbf{E}_S\mathbf{E}_S^T\mathbf{U}_1(\boldsymbol{\theta}_j)\}) \tag{14}$$

where $\boldsymbol{\theta}_j$ represents jth candidate location, $\mathbf{U}_1$ contains the left singular vectors of that location lead field matrix, and $\lambda_{\max}$ is the largest eigenvalue of the bracketed item. Signal subspace is $\mathbf{E}_S = [\mathbf{e}_1, \mathbf{e}_2, ..., \mathbf{e}_D]$ where $\mathbf{e}_i$ with i = 1,2,…,D are normalized eigenvectors of $\overline{\mathbf{R}}$ corresponding to D dominant eigenvalues where their energy is equal or more than a predefined threshold. In this paper, we consider the threshold value about 95%. The orientation of first source $\overline{\mathbf{m}}_1$ is computed using (9) since this method shows more accurate

result than the approach proposed by Mosher and Leahy (according to our simulation results).

In next step, the orthogonal projector for $\mathbf{b}_1 = \mathbf{H}(\overline{\boldsymbol{\theta}}_1)\overline{\mathbf{m}}_1$ that projects onto the left null space of $\mathbf{b}_1$ is defined as

$$\boldsymbol{\Pi}_{\mathbf{b}_1}^{\perp} = \mathbf{I}_M - (\mathbf{b}_1\mathbf{b}_1^T)/(\mathbf{b}_1\mathbf{b}_1^T). \tag{15}$$

Then second source is found as the global maximizer of the following projection metric

$$\overline{\boldsymbol{\theta}}_2 = \max_{\boldsymbol{\theta}}(\lambda_{\max}\{\mathbf{U}_2^T(\boldsymbol{\theta}_j)\mathbf{E}_{2S}\mathbf{E}_{2S}^T\mathbf{U}_2(\boldsymbol{\theta}_j)\}) \tag{16}$$

where $\mathbf{U}_2$ contains the left singular vectors of $\boldsymbol{\Pi}_{\mathbf{b}_1}^{\perp}\mathbf{H}(\boldsymbol{\theta}_j)$, and $\mathbf{E}_{2S}$ is equal to $\boldsymbol{\Pi}_{\mathbf{b}_1}^{\perp}\mathbf{E}_S$. The gain vector for the second source is $\mathbf{b}_2 = \mathbf{H}(\overline{\boldsymbol{\theta}}_2)\overline{\mathbf{m}}_2$, where again source orientation is determined by (9).

At rth iteration, orthogonal projector for the gain vectors found in previous iterations are obtained as

$$\boldsymbol{\Pi}_{\mathbf{B}_{r-1}}^{\perp} = \mathbf{I}_M - (\mathbf{B}_{r-1}\mathbf{B}_{r-1}^T)/(\mathbf{B}_{r-1}\mathbf{B}_{r-1}^T) \tag{17}$$

where,

$$\mathbf{B}_{r-1} = [\mathbf{b}_1, \mathbf{b}_2, ..., \mathbf{b}_{r-1}]. \tag{18}$$

And the rth recursion is performed by following modified cost function

$$\overline{\boldsymbol{\theta}}_r = \max_{\boldsymbol{\theta}}(\lambda_{\max}\{\mathbf{U}_r^T(\boldsymbol{\theta}_j)\mathbf{E}_{rS}\mathbf{E}_{2S}^T\mathbf{U}_r(\boldsymbol{\theta}_j)\}) \tag{19}$$

where $\mathbf{U}_r$ contains the left singular vectors of $\boldsymbol{\Pi}_{\mathbf{B}_{r-1}}^{\perp}\mathbf{H}(\boldsymbol{\theta}_j)$, and $\mathbf{E}_{rS}$ is equal to $\boldsymbol{\Pi}_{\mathbf{B}_{r-1}}^{\perp}\mathbf{E}_S$. The lead field matrix of rth source projected onto the left null space of previously found $(r-1)$ sources has the most correlation with signal subspace projected onto that left null space. The iterations are stopped when the subspace correlation achieved from (19), drops below a given threshold.

Because of good performance of RAP-MUSIC in resolvability of highly correlated brain activity (at least in our simulations), it is exploited in iDMR and the threshold for terminating the iterations is selected to be 0.7.

Proposed Method

The MVB-based methods capability in reconstructing spatio-temporal brain activity has been demonstrated in many publications (Sekihara and Nagarajan 2008; Veen et al. 1997; Sekihara et al. 2001). However, their performance is degraded when dealing with the correlated activity or interference sources.

In this study, the application of indirect dominant mode rejection (iDMR) beamformer in reconstructing correlated neural activity in the presence of interference is investigated, by considering the fact that the performance of iDMR in improving the output SNR in wireless communications is demonstrated by Santos et al. (2007). The main idea of iDMR is to eliminate the cross correlation among the active sources by discarding the nondiagonal elements of source covariance matrix.

In the following the mathematical details of the proposed method are presented. Measurement formulated in (1) can be written as

$$\mathbf{x}(t) = \mathbf{A}\mathbf{s}(t) + \mathbf{n}(t) \tag{20}$$

where $\mathbf{A} = [\mathbf{a}_1, \mathbf{a}_2, ..., \mathbf{a}_L]$ with $\mathbf{a}_i = \mathbf{H}(\mathbf{q}_i)\mathbf{m}(\mathbf{q}_i)$, and $\mathbf{s}(t) = [s_1(t), s_2(t), ..., s_L(t)]^T$. Then, the spatial correlation matrix of the measurement is formulated as

$$\mathbf{R} = \mathbf{A}\mathbf{C}(s)\mathbf{A}^T + \mathbf{A}\mathbf{C}_{ns} + \mathbf{C}_{sn}\mathbf{A}^T + \mathbf{Q} \tag{21}$$

where $\mathbf{C}(s)$ is covariance matrix of sources, $\mathbf{Q}$ is covariance matrix of noise, $\mathbf{C}_{ns}$ and $\mathbf{C}_{sn}$ are correlation matrices of noise with sources and sources with noise. By assuming that noise exists in the null space of the sources, the above expression can be approximated as

$$\overline{\overline{\mathbf{R}}} = \mathbf{A}\mathbf{C}(s)\mathbf{A}^T + \mathbf{Q}. \tag{22}$$

Now simply the $\mathbf{C}(s)$ can be achieved

$$\mathbf{C}(s) = \mathbf{A}^{\dagger}(\overline{\overline{\mathbf{R}}} - \mathbf{Q})\mathbf{A}^{T\dagger} \tag{23}$$

where † denotes the pseudo-inverse. In practice, $\overline{\mathbf{R}}$, estimated in (5), is used instead of $\overline{\overline{\mathbf{R}}}$. In the next step, only the diagonal entries of $\mathbf{C}(s)$ that are the variance of the sources are preserved and other entries are replaced with zero. By substituting the modified source covariance matrix $\overline{\mathbf{C}}(x)$ in (22) the modified measurement covariance matrix is attained as

$$\widehat{\mathbf{R}} = \mathbf{A}\overline{\mathbf{C}}(x)\mathbf{A}^T + \mathbf{Q} \tag{24}$$

And substituting the $\widehat{\mathbf{R}}$ into (4) gives the following weight expression for iDMR approach

$$\mathbf{W}_{iDMR}(\mathbf{q}_0) = \widehat{\mathbf{R}}^{-1}\mathbf{H}(\mathbf{q}_0)\left(\mathbf{H}^T(\mathbf{q}_0)\widehat{\mathbf{R}}^{-1}\mathbf{H}(\mathbf{q}_0)\right)^{-1} \tag{25}$$

As the final step, the iDMR beamformer is extended to an eigenspace projected beamformer by projecting the weight matrix expressed in (25) onto the signal subspace

$$\mathbf{W}_{eiDMR}(\mathbf{q}_0) = \mathbf{E}_S\mathbf{E}_S^T\mathbf{W}_{iDMR}(\mathbf{q}_0). \tag{26}$$

Brain activity is visualized based on the spatial filter output power that is computed by

$$P_Z^{iDMR}(\mathbf{q}_0) = \lambda_{\max}\{\mathbf{W}_{iDMR}^T(\mathbf{q}_0)\overline{\mathbf{R}}\mathbf{W}_{iDMR}(\mathbf{q}_0). \\ (\mathbf{W}_{iDMR}^T(\mathbf{q}_0)\mathbf{Q}\mathbf{W}_{iDMR}(\mathbf{q}_0))^{-1}\}. \tag{27}$$

Table 1 Outline of the iDMR algorithm

i	Estimate matrix $\overline{\mathbf{R}}$ using Eq. (5) and use it instead of $\overline{\overline{\mathbf{R}}}$
ii	Estimate matrix $\mathbf{A}$ using RAP-MUSIC
iii	Estimate noise covariance matrix $\mathbf{Q}$
iv	Compute $\overline{\mathbf{C}}(x) = diag(\mathbf{A}^{\dagger}(\overline{\overline{\mathbf{R}}} - \mathbf{Q})\mathbf{A}^{T\dagger})$
v	Compute $\hat{\mathbf{R}} = \mathbf{A}\overline{\mathbf{C}}(x)\mathbf{A}^T + \mathbf{Q}$
vi	Compute $\mathbf{W}_{iDMR}(\mathbf{q}_0) = \hat{\mathbf{R}}^{-1}\mathbf{H}(\mathbf{q}_0)\left(\mathbf{H}^T(\mathbf{q}_0)\hat{\mathbf{R}}^{-1}\mathbf{H}(\mathbf{q}_0)\right)^{-1}$

The matrix $\mathbf{A}$ is derived using RAP-MUSIC method such that for L diploes matrix $\mathbf{A}$ is equal to $\mathbf{B}_L$ in (18). The Table 1 outlines the iDMR algorithm.

iDMR technique requires knowledge the noise covariance matrix. $\mathbf{Q}$ may be estimated from data that is known to be source free, such as pre-stimulus data.

In the next section, by suitable simulations is attempted to as complete as possible evaluations regarding the performance of the iDMR are presented.

Performance Evaluations

Numerical Experiments

We explored the performance of iDMR on both EEG and MEG data. Forward solution was computed for both types of data by Brainstorm software.[1] For EEG case, the brain volume extracted from Colin27 MRI was segmented into 15,002 vertices with 2–5 mm resolution. Herein, we used a HydroCel Geodesic Sensor Net (HCGSN) with N = 256 electrodes and represented head volume conductor by three shell spherical head model (Mosher and Leahy 1999; Berg and Scherg 1994). Spheres were centered at [x, y, z] = [1.76, 1.19, 53.83] mm when the outer, middle, and inner shells radiuses were 97.4, 80.84, and 75.97 mm, respectively. The conductivities of three shells were set to [0.33, 0.0042, 0.33] S/m. For MEG case, we used the subject anatomy related to the data that was used for evaluation and is available in Brainstorm toolbox. Gain matrix for 15,016 vertices and with "overlapping sphere" head model was calculated. All spatial coordinates in this paper are expressed in CTF coordinate system whose origin is midway on the line joining left pre-auricular point[2] (LPA) and right pre-auricular point (RPA) and the x-, y-, and z axes are oriented along

the back–front, right–left, and bottom–top directions, respectively.

Some preliminary definitions are required to proceed. We define the simulated data SNR and correlation between sources as follows

$$SNR = 10\log\left(\frac{tr(\mathbf{A}_s^T\mathbf{A}_s)}{tr(\mathbf{n}^T\mathbf{n})}\right) \tag{28}$$

$$corr = \frac{\langle \mathbf{s_1}, \mathbf{s_2}\rangle}{\|\mathbf{s_1}\|_2\|\mathbf{s_2}\|_2} \tag{29}$$

where matrix $\mathbf{A}_s$ is equal to $\sum_{i=1}^{L}\mathbf{H}(\mathbf{q}_i)\mathbf{m}(\mathbf{q}_i)s(\mathbf{q}_i)$ for all time points, s_1 and s_2 are time course of sources 1 and 2, respectively, $\mathbf{n}$ is noise matrix for all time points, $\langle,\rangle$ denotes inner product, and $\|.\|_2$ represents Euclidean norm. Notice that we take into account the interference source in the SNR definition.

Comparative Performance Evaluations

In the following, we aim firstly to explore the ability of the iDMR with/without source covariance diagonalization and with/without signal space projection in comparison to conventional MVB. Then, iDMR performance in comparison to MPZ is evaluated in a difficult scenario. Finally, proposed method is applied on the real AEF data containing highly correlated sources.

For simulation data and for iDMR method, activity map on the cortex is derived by putting a threshold on maximum power of this method. This threshold value is considered 0.9, meaning vertices with more than 0.9 Pmax activity are shown with red color.

In all scenarios, we computed $\overline{\mathbf{R}}$ across all trials from post stimulus period. For time course reconstruction, we applied weight matrix to post stimulus data averaged across trials because it had high SNR and averaging acts as a low pass filter.

Evaluation of iDMR Performance in a Z-Plane

Before comparing iDMR with MPZ, in this section, we plane to compare iDMR performance with a few other beamformers and find the main reason for its success. MVB and eigenspace-projection MVB (eMVB) are two of those methods. In eMVB, the spatial filter computed using (4) is projected onto signal subspace by production of $E_sE_s^T$ with $\mathbf{W}_{MVB}$ and then projected $\mathbf{W}_{eMVB}$ is used for source localization and time course reconstruction. By comparing MVB and eMVB, we can understand the role of

---

[1] BrainStorm, Matlab Toolbox. http://neuroimage.usc.edu/brainstorm /2017.

[2] A point of the posterior root of the zygomatic arch lying immediately in front of the upper end of the tragus.

eigenspace-projection on MVB performance. By comparing MVB with proposed method, one can observe the effect of iDMR covariance matrix on MVB results. For a detailed exploration, we also run simulation for "undiagonal iDMR" method in which everything is the same as iDMR but the difference is that we keep all elements of the source covariance matrix (not decorrelated). Comparison between iDMR and undiagonal iDMR can better show and highlight the significance of modified source covariance matrix. One maybe wants to see the effect eigenspace-projection on iDMR performance, so we consider the eiDMR as fourth method for comparison.

In this section, an EEG simulation is implemented. Our reconstruction area was a z-plane: z = 90 mm to be better shown the spatial resolution. This plane was defined by -5 cm $\leqslant x \leqslant 5$ cm and -5 cm $\leqslant y \leqslant 5$ cm the reconstruction interval was 1 mm in the x and y directions, totally 10,201 candidate locations. Two highly correlated sources (corr = 0.9) were positioned at $[-26, 1, 90]$ mm and $[24, 1, 90]$ mm and interference source was activated at $[-1, -33, 90]$ mm. All three sources had equal orientation unit-norm vectors, $[1, 1, 1]/\sqrt{3}$. Totally, 300 trials were generated each of which at a 1-ms interval from -1 to 1 s. Each trial comprises 1 s of rest (pre-stimulus) followed by 1 s activity (post-stimulus). Pre-stimulus contains noise to which interest and interference activities were added in post-stimulus. In this study, we used the method of Yeung et al. (2004) to generate the trials noise (not using simple white noise). Noise component n(r,j) on the jth channel at rth trial, which was added to the temporal file of the active sources, was generated by summation of 50 sinusoidal signals with increasing frequencies as follows:

$$n(r, j) = \sum_{i=1}^{50} A_{f_i} \sin\left(\frac{2\pi k f_i}{f_s} + \phi_{n,i} \right) \tag{30}$$

where $f_i = f_{i-1} + f_{rand}$ with $f_0 = 0 Hz$ and f_{rand} is a random variable uniformly distributed between 0 and 2.5, $\phi_{n,i}$ is a random phase uniformly distributed between 0 and 2π radians, and A_{f_i} represents amplitude of sinusoid signals decreasing exponentially with frequency and is given by

$$A_{f_i} = \exp(-\lfloor f_i \rfloor / 25) \tag{31}$$

where $\lfloor f_i \rfloor$ represents f_i rounded down to the nearest integer.

Our signal is an event related potential (ERP) type the SNR of which is usually in the range of 3–5 dB, thus we defined amplitude of noise so that the ERP SNR became 4 dB. The ERP signal is shown in Fig. 1d. The **Q** was computed across all trials from pre stimulus period.

The cross-section of the source activities on the line y = 1 mm and y = −33 mm computed by eiDMR, iDMR, undiagonal iDMR, eMVB, and MVB are illustrated in Fig. 1a–c. If we define mean of the full-width–half-maximum

(FWHM) for two correlated sources as a metric for assessing the spatial resolution, the values of which for eiDMR, iDMR, eMVB are 7, 7, and 42 mm, respectively. This metric for MVB and undiaginal iDMR is not computable because, as can be seen from Fig. 1c, their output powers never reach to their half-maximum value. Based on Fig. 1c, the eMVB gives better spatial resolution but less output SNR, in comparison to MVB and undiagonal iDMR. However, the more output SNR of MVB and undiagonal iDMR is the result of more noise in their spatial filter output. Based on Fig. 1a, c, proposed method outperforms the others in both aspects spatial resolution and output SNR. These superiorities are the results of better noise cancellation and accurate time course reconstruction. For the third source, Fig. 1b, all five algorithms present well results but iDMR obtains the highest output SNR. The eiDMR presents the same performance as iDMR, meaning source decorrelation is sufficient and there is no need for eigenspace-projection.

Also, the image of source power on the plane z = 90 mm is shown in Fig. 2 for aforementioned methods. As seen, iDMR completely discriminates two sources and together with eiDMR obtain the most concentrated power spectrum. Whereas, other three methods show two sources with less power and more spatial blur. Proposed method shows third source with more intense red color because, as shown in Fig. 3, its time course has more nonzero values, thereby corresponding output power is more. Difference between the images of the iDMR and undiagonal iDMR verifies the significance of eliminating the sources cross-correlation from measurement covariance matrix.

Estimated time courses for all sources are presented at Fig. 3. As it is evident, proposed method fully reconstructs the time courses in aspects of shape and amplitude. Additionally, clearer time courses are achieved by iDMR. As a result, iDMR/eiDMR can provide higher SNR than the other methods. Reconstructed time courses of correlated sources by other methods are completely distorted and too much noisy. In contrast to iDMR/eiDMR, spatial filter pass bands of other methods allow contribution of noise to the time course of desired source, resulting in time course suppression and distortion, which in turn leading to decreased SNR. Another advantage of accurate time course estimation is that iDMR can be exploited as a localizer with high temporal resolution in order of 1 ms.

For understanding the main reason for iDMR high level performance, it is better to mention to some facts that can be found from shown figures and formulations of the algorithm. The one is eigenspace-projection has no role in iDMR performance. The only difference between iDMR and undiagonal iDMR is using decorrelated source covariance matrix in iDMR. The only difference between MVB and undiagonal iDMR is using less noisy expressions in the latter method data covariance matrix because there are two noisy
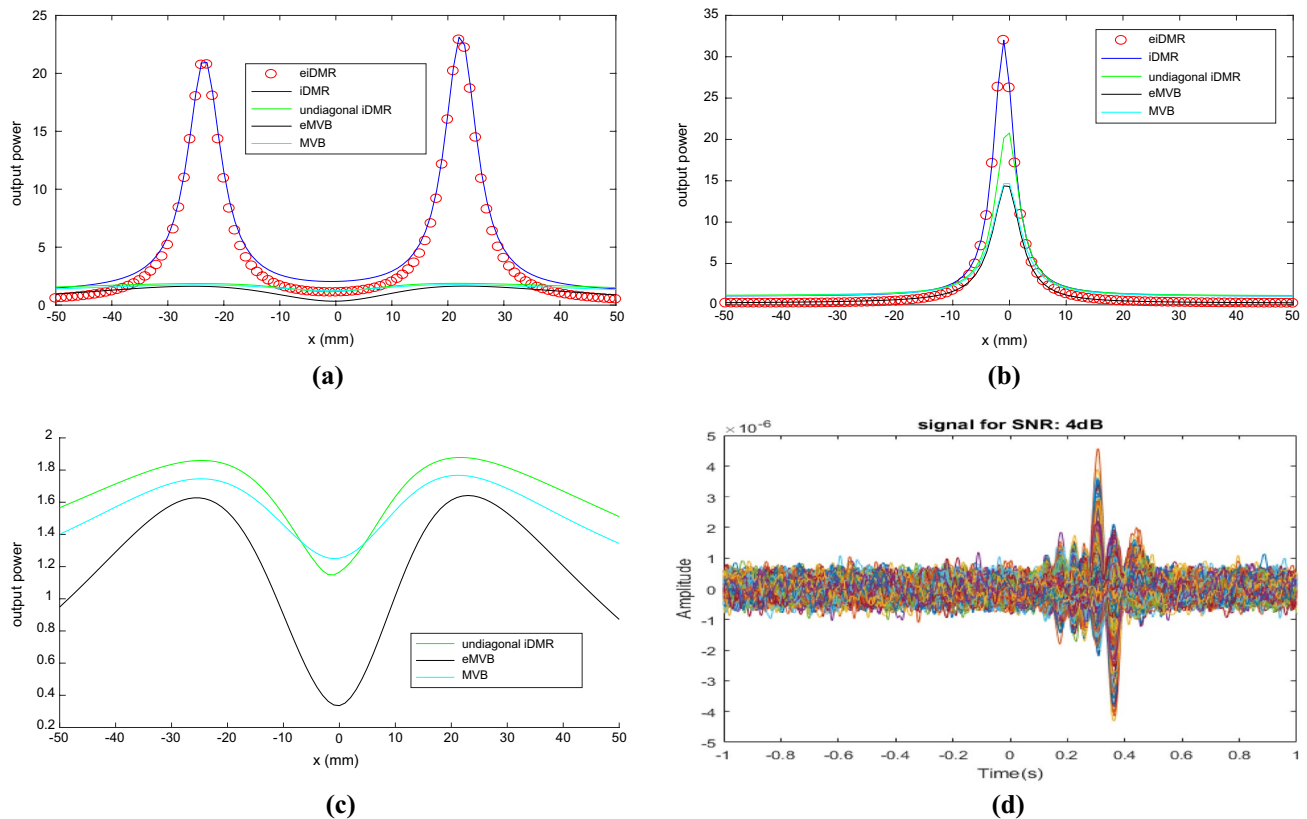
(a)

(b)

(c)

(d)

Fig. 1 The cross-section of the source activities on the line **a** y = 1 mm and **b** y = −33 mm computed by eiDMR, iDMR, undigonal eiDMR, eMVB, and MVB methods, when two highly correlated and one interference sources are located at [−26, 1, 90] mm, [24, 1, 90] mm and [−1, −33, 90] mm. For better visualization purpose, results of undigonal eiDMR, eMVB, and MVB methods are shown in **c**. The simulated signal at SNR = 4 dB is plotted in **d**

sentences $\mathbf{A}\underline{\mathbf{C}}_{ns}$ and $\mathbf{C}_{sn}\mathbf{A}^T$ in earlier method sample covariance matrix $\overline{\mathbf{R}}$ (assuming matrix $\mathbf{A}$ is constructed correctly). Based on the similar results of MVB and undiagonal iDMR and also superior performance of iDMR than undiagonal iDMR, we can conclude that the main reason for high level performance of iDMR and the way for increasing MVB performance to that of iDMR is using data covariance matrix in which sources are decorrelated.

Evaluation of iDMR Performance in Comparison to MPZ Algorithm

In this scenario, we aim to investigate the performance of our proposed method versus another well-known technique for correlated sources localization, MPZ technique, in a somewhat difficult situation. For generation of event related field data, four sources were activated; two sources with high correlation (corr = 0.9) at left and right primary auditory cortex area, one source at somatosensory area, and the interference source at the frontal part of the brain left lobe. Each source was oriented normal to the cortex. Totally, 400 trials each with 400 samples were generated

with sampling frequency of 600 Hz. For simulation noise, we used the resting state MEG recordings which is available in Brainstorm download page and using it for research purpose needs written consent from the MEG Lab. It was based on an eyes open resting recordings of one subject and recorded at the Montreal Neurological Institute in 2012 with a CTF MEG 275 system. Experiment included two runs of 10 min of resting state recordings with sampling frequency of 2400 Hz. Details of this dataset can be found in the tutorial "MEG resting state and phase-amplitude coupling" at Brainstorm tutorial web page. Without missing desired information and for decreasing computational cost, we downsampled data to 600 Hz. This dataset was processed based on the Brainstorm tutorial related to this data (Tadel et al. 2011). We considered the one of the runs for generation ERF data and the other one for computing noise covariance matrix. For signal generation, noise amplitude was set so that SNR was equal to 0dB for averaged ERF data. This amplitude setting was also applied to other rest data which is used for noise covariance matrix estimation. The information of rest data, run1, such as subject anatomy, cortex and channel file were used
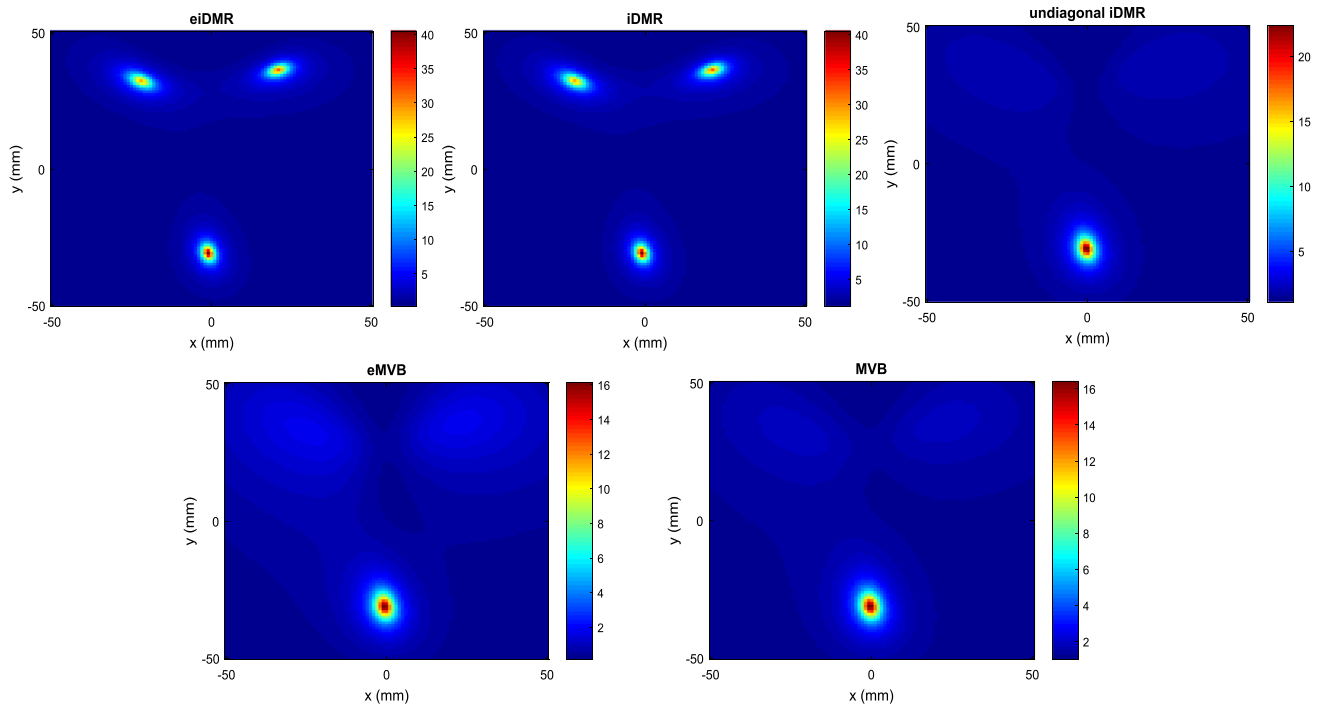
Fig. 2 The image of source power on the plane z = 90 mm for eiDMR, iDMR, undiagonal eiDMR, eMVB, and MVB, when two sources with correlation of 0.9 are located at [−26, 1, 90] mm and [24, 1, 90] mm and one interference source (uncorrelated with two others) is located at [−1, −33, 90] mm

for computing lead field matrices. The generated averaged ERF data can be seen from Fig. 4.

Power map results are illustrated in Fig. 5. For MPZ, the found location at each iteration is indicated by a green point. True source locations in the brain right and left lobes are labeled as GT_R and GT_L. Localization results of iDMR for the right and left lobes are indicated with iDMR_R and iDMR_L, respectively. By considering that four sources are activated, MPZ is implemented for six iterations. In Fig. 5, the location of found source in each iteration is indicated as green point. As it is obvious, proposed method can accurately estimate active source locations with the most spatial resolution. MPZ algorithm only can localize somatosensory area source (iteration one) correctly. Reconstructed time courses are plotted in Fig. 6. For MPZ algorithm, the time courses of sources localized at iterations 1–4 are plotted.

Proposed method can perfectly reconstruct time courses in aspects of shape and pick to pick amplitude. MPZ approach cannot estimate true locations and thereby cannot make a spatial filter which is specific for active sources. As a bad result, undesired source activities and noise can contribute into desired source activities and so reconstructed time courses are far from the true ones in aspects of shape and amplitude. The bad effects of interference source are evident in MPZ time courses. The single pseudo-Z score for six iterations is shown in Fig. 5 with a bar plot. Based on

these z-scores, one may interpret that two or at most three active sources generate ERF data and only considers and reports results related to the sources localized at iterations 1–3, whereas we now that the number of active sources is four.

Two reasons can be posed for superiority of iDMR in comparison to MPZ. The first one is that iDMR uses RAP-MUSIC algorithm for source detection whereas MPZ employs pseudo-Z score which is MVB-based power localizer. Therefore, iDMR in its recursive implementation can find more accurate locations for active sources, due to less sensitivity of RAP-MUSIC to highly correlated sources. The second one is that iDMR results are achieved by two steps processing, RAP-MUSIC and then MVB-based power localizer. The information of first step helps MVB to compensate its weakness point (missing highly correlated sources). Also, it is possible that RAP-MUSIC presents locations around the true locations not exact locations. In this situation, MVB-based power localizer tries to enhance first step performance and present more accurate information. In addition, we define a threshold metric for terminating RAP-MUSIC algorithm the value of which is 0.7, thereby it is possible that RAP-MUSIC finds more sources than true ones. In this situation, again, MVB-based power localizer by its high spatial resolution can focus on true locations (for observing the two last cases, we address enthusiastic readers to real AEF data
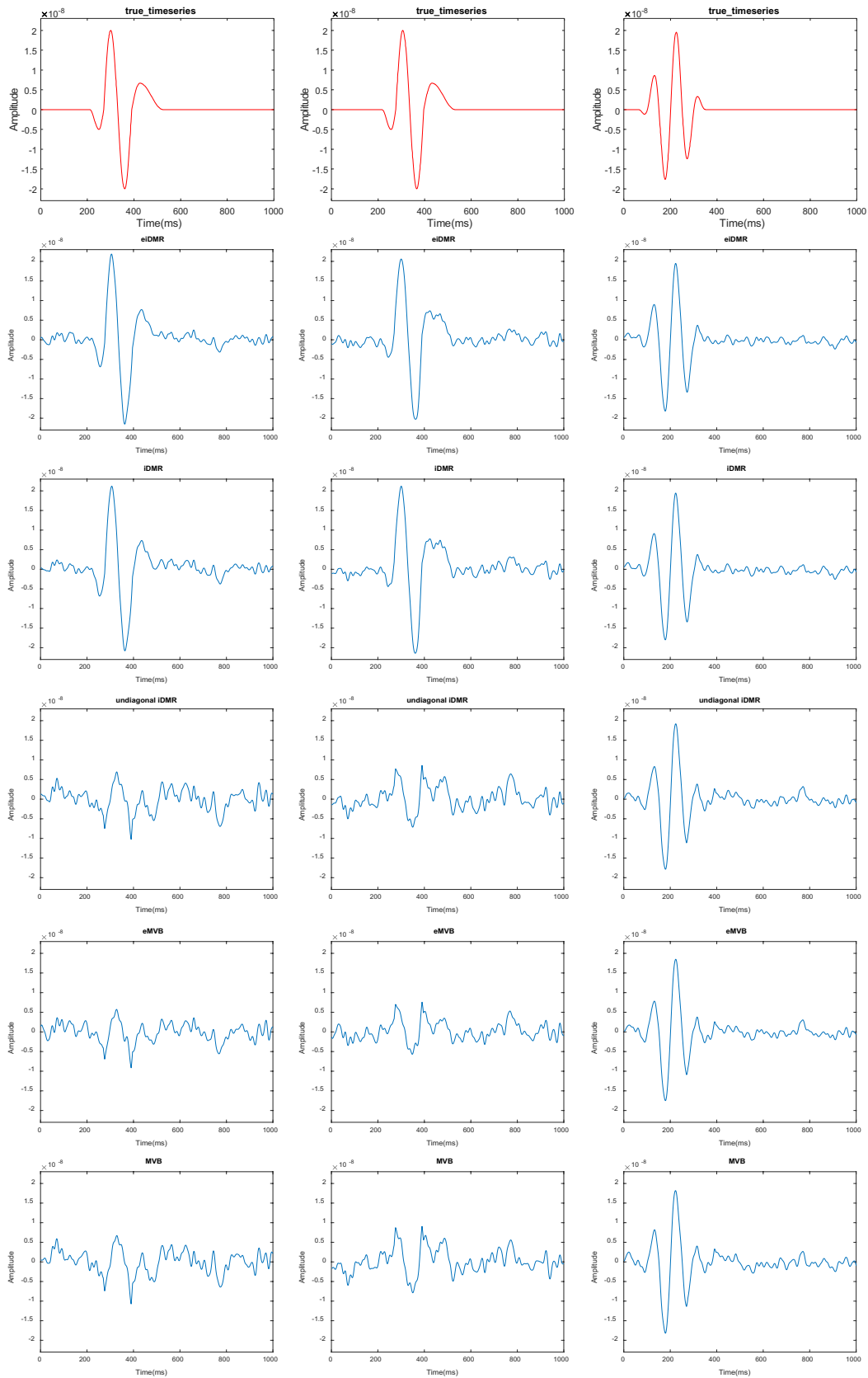
◄**Fig. 3** For "Evaluation of iDMR performance in a Z-plane" scenario: estimated time courses by eiDMR, iDMR, undiagonal iDMR, eMVB, and MVB approaches for correlated sources (first and second columns) and interference source (third column). True time courses are shown in red color

analysis scenario). Overall, we can say that these two steps are necessary and complement each other.

In the following, we applied iDMR method for localization of data when data trial number varied from 20 to 400 in steps of 60 to evaluate the effect of number of trials on the iDMR performance. The cortex activity map is shown in Fig. 7.

Although, for low trial numbers, the iDMR cannot place active sources in their true locations, it provides accurate results for high number of trials. When the number of trials is low, a stable and accurate data covariance matrix cannot be provided. As a result, estimated signal subspace would be far from true signal subspace which in turn leads to decrease the RAP-MUSIC ability for finding active locations. Therefore, iDMR performance is deteriorated. Low trial number is not only a problem for iDMR. Every localization method relying on the data covariance matrices needs to have enough trials for suitable estimation of the data covariance matrix.

Evaluation of iDMR with Real AEF Data

To test performance of the iDMR with experimental data, AEF dataset which is available from the BrainStorm toolbox[1] was analyzed. This dataset was acquired from one subject and with two acquisition runs of 6 min each. Subject stimulated binaurally with intra-aural earphones (air tubes + transducers). Each run contains 200 regular (standard) beeps (440 Hz) 40 easy deviant beeps (554.4 Hz, 4 semitones higher). Data acquisition was done at 2400 Hz, with a CTF 275 system, subject in sitting position. This data was recorded at the Montreal Neurological Institute in December 2013. Without losing desired information and for easier analysis on a regular computer, data was downsampled to 600 Hz.

We preprocessed data using Brainstorm software, based on tutorials provided for this dataset and are available on this software web site (Tadel et al. 2011). Also, we used information of this dataset for computing lead field matrices. We only used first acquisition run and data related to standard beeps because of having more epochs. Used dataset which was averaged over 200 trials is plotted in Fig. 8. Empty room recording, 30 s long, was used for noise covariance estimation.

Regarding that, eye blinks and movements, muscle artifacts were removed with SSP (Signal-Space Projection), one delicate point should be taken into consideration. Since the signal-space projection modifies the signal

vectors originating in the brain, it is necessary to apply the projection to the forward solution in the course of inverse computations. Hence, we applied SSP projectors to lead field matrices and then performed first step of iDMR, RAP-MUSIC. Then, for generating of iDMR data covariance matrix, we also employed projected noise covariance matrix.

The RAP-MUSIC finds seven sources, locations of which are shown in Fig. 9a, b. As one can see from Fig. 9, RAP-MUSIC over-selects active sources, meaning finds seven sources when there are two active areas, left and right primary auditory cortex. This is because of the threshold value, 0.7, which is lower than it is required. In addition, RAP-MUSIC does not position sources in their locations but does around 2–4 cm far from those. Based on the RAP-MUSIC results, the iDMR data covariance matrix is constructed. Then this matrix is uploaded in Brainstorm for localization purpose.

The results of iDMR power maps, are shown in Fig. 9c, d. In contrast to RAP-MUSIC, iDMR can find active locations in primary auditory cortex. This result verifies this idea that even if over-selection or misplacing or both of them (as is the case for this scenario) occur for RAP-MUSIC, second step of iDMR, power based localizer of MVB, can compensate it and present more accurate results. As a result, it can be interpreted that iDMR is not so sensitive to hyper parameter of RAP-MUSIC, threshold value for algorithm termination. However, we offer setting termination value to 0.7 because value too larger (for example 0.9) may be cause under-selection phenomena to occur by RAP-MUSIC. The under-selection can degrade second step performance of iDMR because we know that MVB-based localizers only can detect sources information of which exist in data covariance matrix. However, as real dataset demonstrates, over-selection which is a consequence of lower threshold value is not as destructive as under-selection.

Time courses of left and right primary auditory cortex are plotted in Fig. 9e, f. Although, the responses of right and left auditory cortices are highly correlated, the right response is not as strong as left one. This fact also can be observed in power map results, Fig. 9c, d. These binaural auditory stimulations should be generating similar responses in both left and right auditory cortices at early latencies. Possible explanations for this observation maybe justified by possible reasons presented by brainstorm web page:

(1) The earplug was not adjusted on the right side and the sound was not well delivered.
(2) The subject's hearing from the right ear is impaired.
(3) The response is actually stronger in the left auditory cortex for this subject.
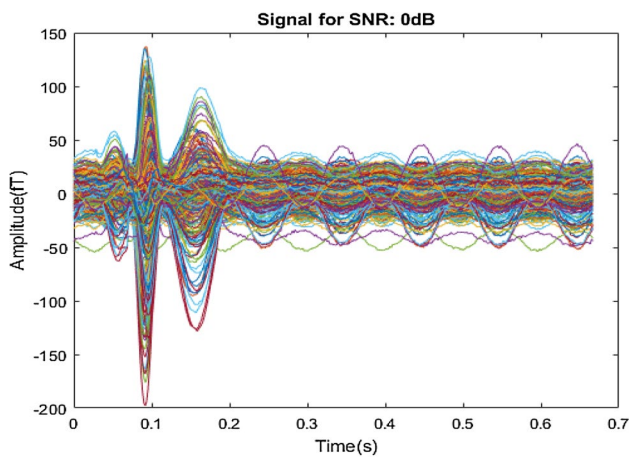(4) The orientation of the source makes it more difficult for the MEG sensors to capture.

Fig. 4 The averaged ERF signal at 0 dB, when two highly correlated sources at left and right primary auditory cortex and one uncorrelated source in somatosensory area and one interference source in frontal part of left lope are activated

For real data, noise covariance and gain matrices were needed to be projected onto the null-space of data artifacts. Hence, we computed the iDMR data covariance matrix and then uploaded it into brainstorm software. After that, we applied the beamformer in the brainstorm which carried out the projection. The colormap scales are based on the brainstorm scale (not normalized to scale 1).

The Fig. 9c, d were plotted in brainstorm by constraint orientation approach. The widespread scatter in the localization results of iDMR is due to the orientation constraint on the dipoles orientations. Each value on the cortex should be interpreted as a vector, oriented perpendicular to the surface. Because of the brain's circumvolutions, neighboring sources can have significantly different orientations, which also causes the forward model response to change quickly with position. As a result, the orientation-constrained solution can produce solutions that vary rapidly with position on the cortex resulting in the noisy and disjointed appearance (Tadel et al. 2011).

For data exploration, orientation-constrained solutions may be a good enough representation of brain activity, mostly because it is fast and efficient.
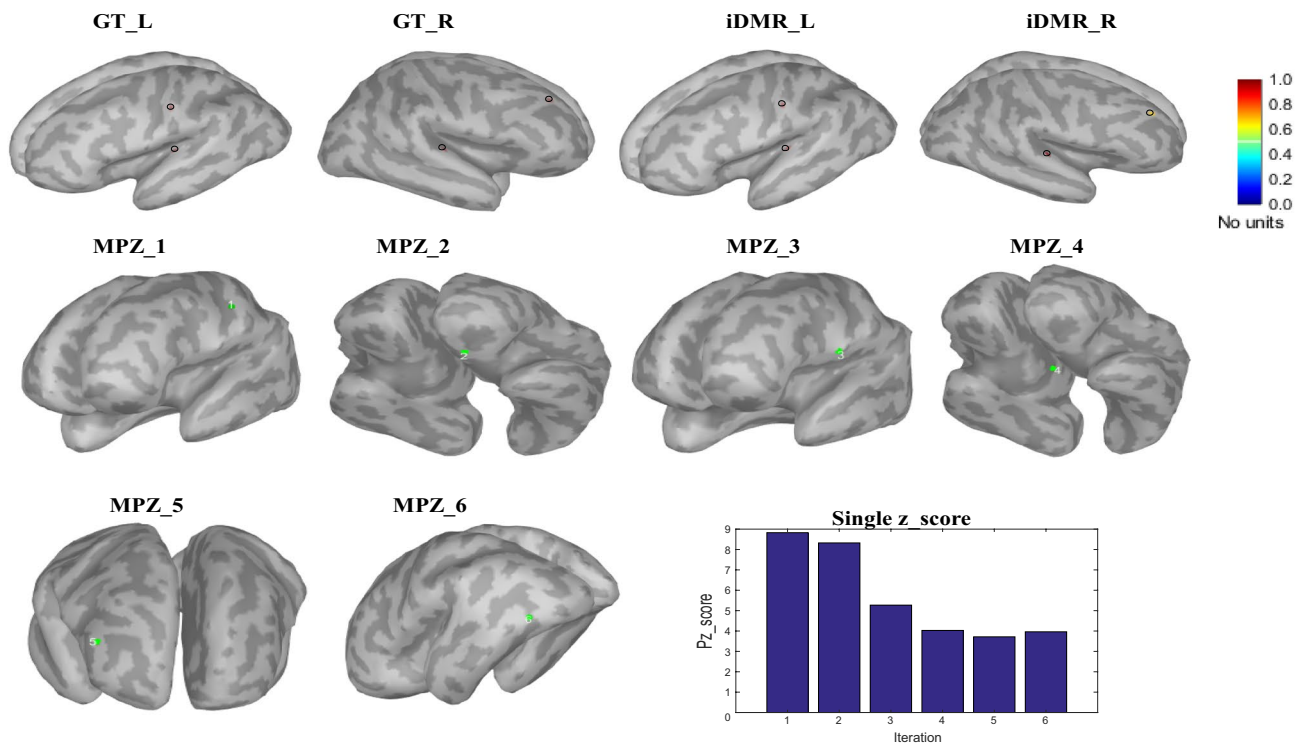
However, simulation results and real data one guarantee the applicability of iDMR for localization, time course reconstruction of highly correlated sources.

Fig. 5 For "Evaluation of iDMR performance in comparison to MPZ algorithm" scenario: power computed by iDMR is mapped on the left (iDMR_L) and right (iDMR_R) lobes. MPZ_i shows location of detected source in iteration *i*. Scores of single pseudo *z* for six iterations are shown by bar plot. True locations of active sources are shown with labels GT_L and GT_R. iDMR can successfully find active sources locations while MPZ can only find somatosensory area source. The results of bar plot indicates that single z_score can only inform about existence of at most three active sources while there are four active ones. The power of vertices are divided by the maximum power so the color-bar represents no unit for its values
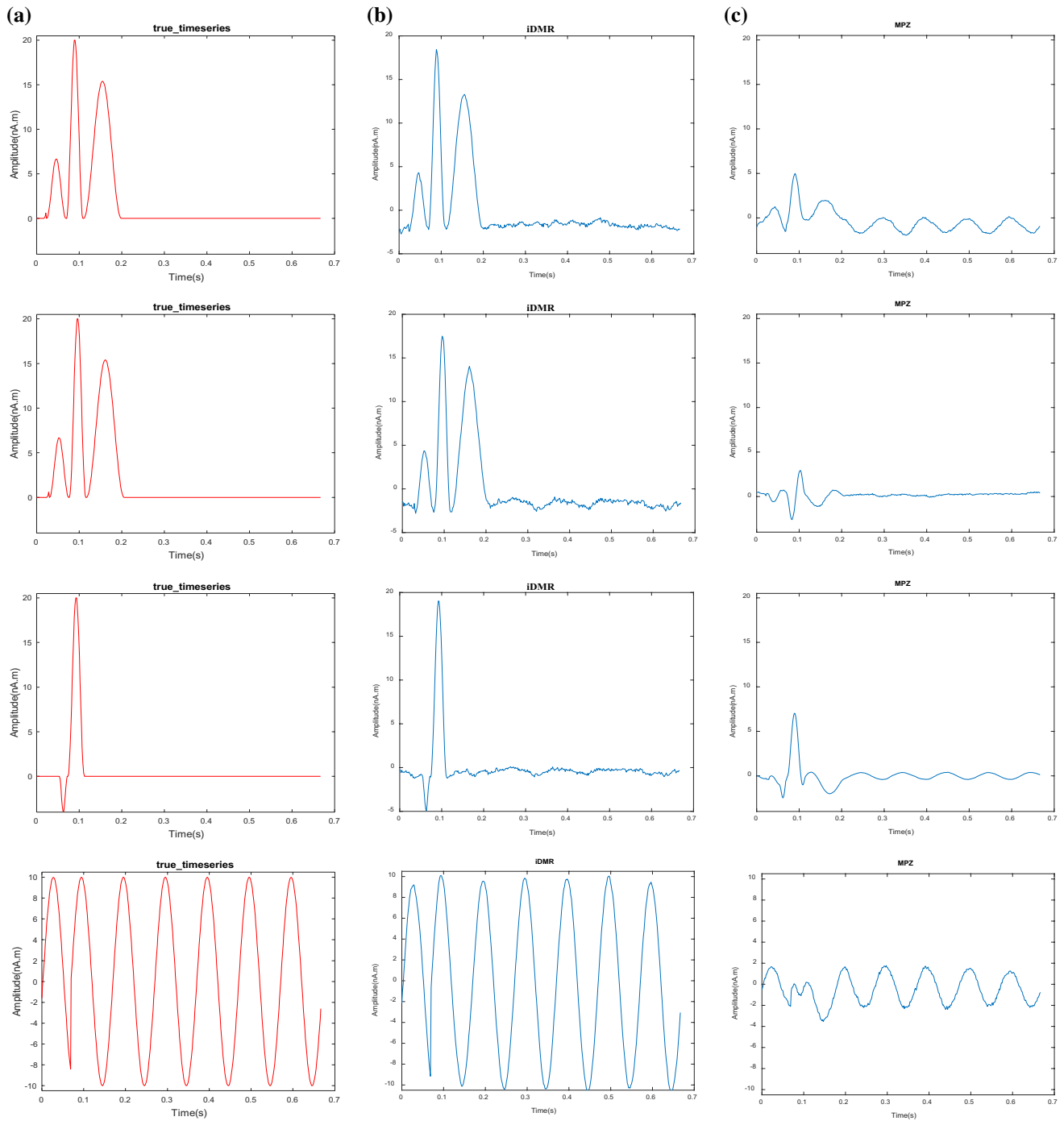
Fig. 6 For "Evaluation of iDMR performance in comparison to MPZ algorithm" scenario: estimated time courses by **b** iDMR and **c** MPZ approaches for correlated sources (first and second rows), somatosen- sory source (third row) and interference source (fourth row). True time courses are shown with red color (**a**)

In the following, we applied iDMR method for localiza- tion of real data when data trial number varied from 20 to 200 in steps of 60 to evaluate the effect of number of trials on the iDMR performance. The cortex activity map is shown in Fig. 10. For low trial number, iDMR fails in localization

of AEF data whereas by increasing the trial number iDMR performance is increased.

The real data is low SNR itself. Thus, it is needed to com- pute the data covariance matrix across many trials to achieve a stable and more accurate data covariance matrix and there- fore more accurate signal subspace for RAP-MUSIC. Hence,
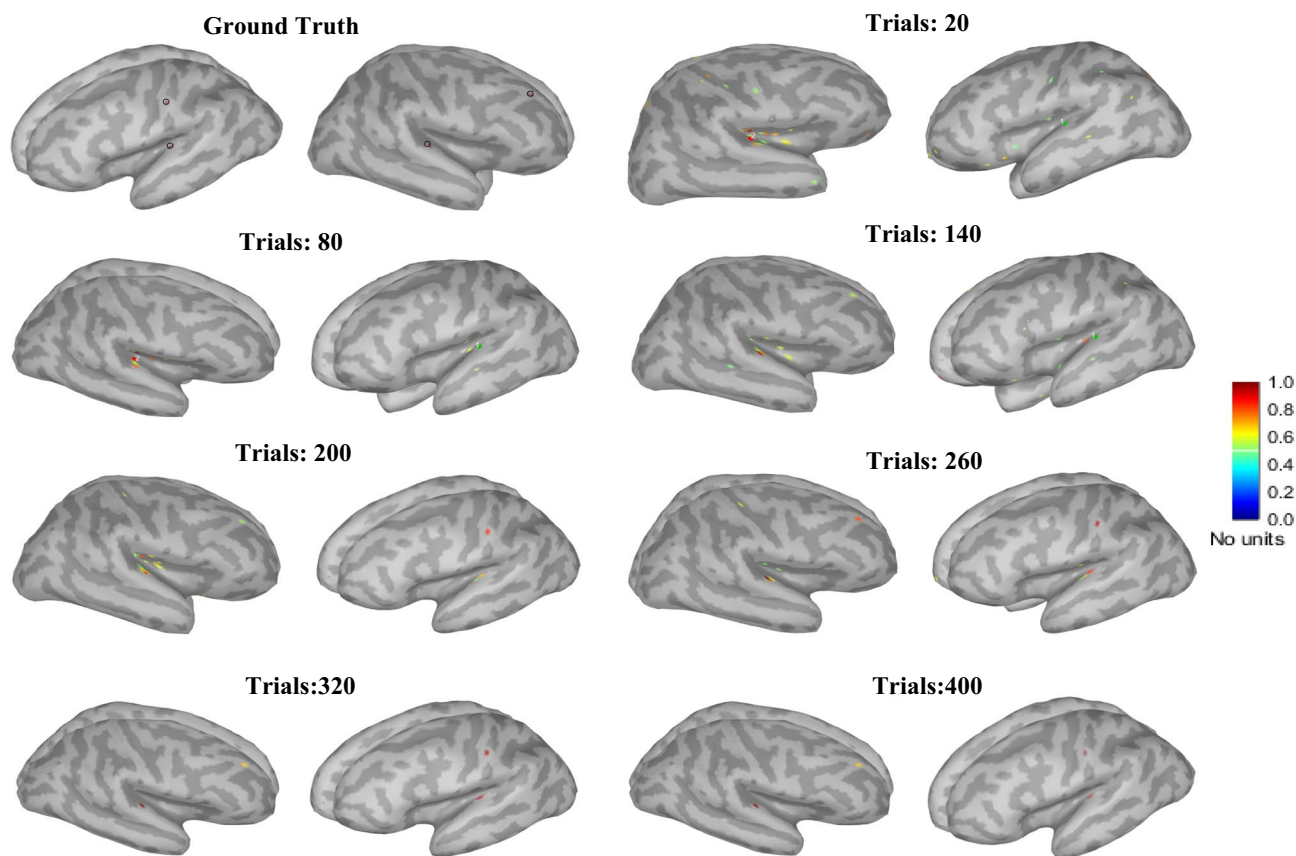
Fig. 7 Investigation of iDMR performance in localization of simulation data of scenario 2 when number of trials varies from 20 to 400 in steps of 60. Ground truth is shown for comparison purpose. The power of vertices are divided by the maximum power so the color-bar represents no unit for its values
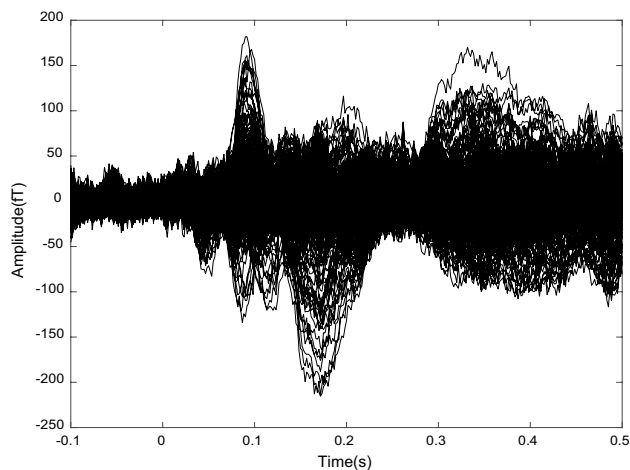

Fig. 8 AEF dataset related to standard beeps. This dataset is recorded with a CTF 275 system and averaged over 200 trials

it is better not only for iDMR but also for other methods using data covariance matrix to employ more trials and observations, as possible.

Discussion

Our aim in this study was to apply the indirect dominant mode rejection (iDMR) approach to data produced by activation neural sources and to investigate its performance while complicated conditions such as existence of correlated and interference sources were taken into account. According to the results of implemented scenarios, iDMR shows its superiority to traditional beamformers MVB and eMVB and also new version one MPZ which is developed for dealing with correlated sources.

We implemented scenario "Evaluation of iDMR performance in a Z-plane" to understand the key reason for high level performance of proposed method. We understood the results of iDMR were the same as that of eiMR and also the results of undiagonal iDMR were similar to that of MVB. Therefore, we concluded that the main reason for excellent performance of iDMR and also the way for increasing the MVB perfprmance to that of iDMR is using data covariance, for weight matrix, in which source covariance matrix is decorrelated.
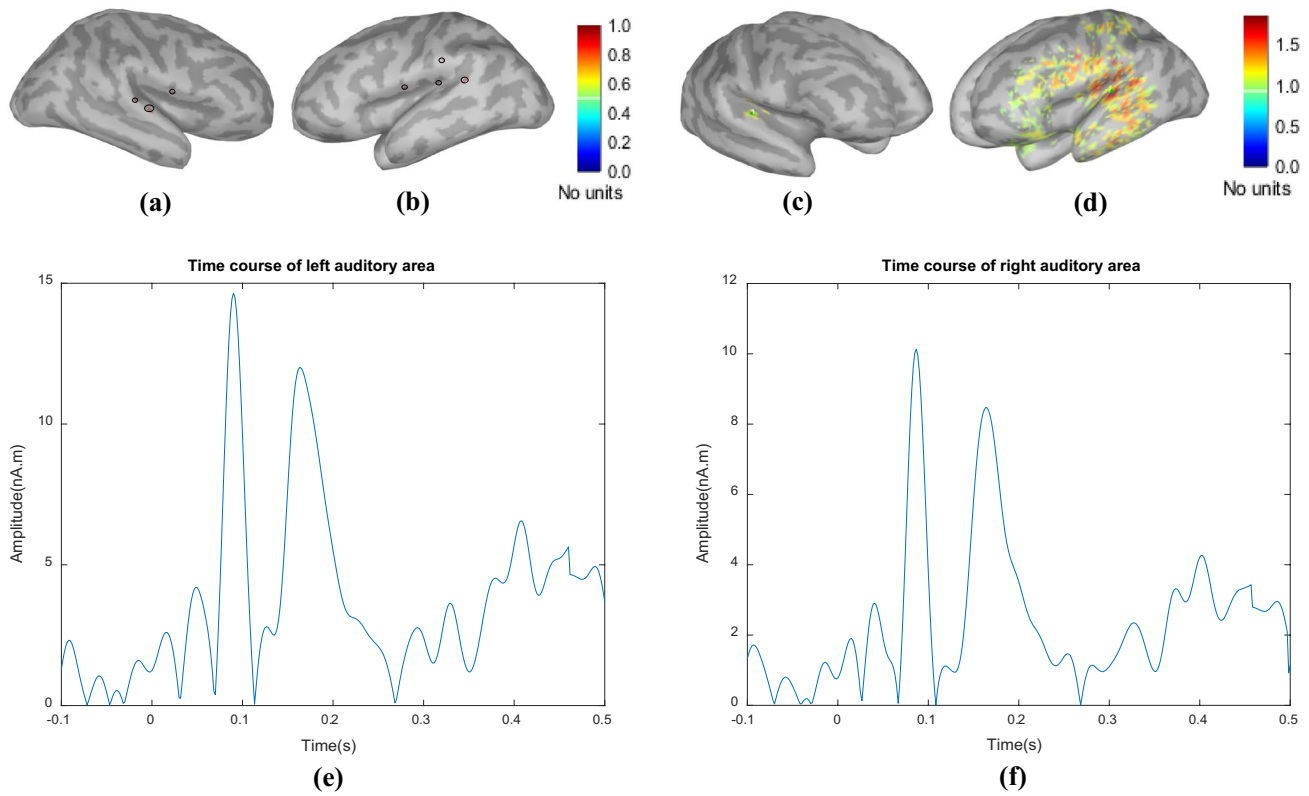
Fig. 9 For "Evaluation of iDMR with real AEF data" scenario: **a** and **b** illustrate the sources found by RAP-MUSIC for left and right brain hemispheres. **c** and **d** Present localization results of iDMR for left and right auditory area. **e** and **f** Plot the absolute of time courses of left and right auditory areas. Locations of left and right auditory sources are indicated by green points. For auditory data, color-bar values represent the power localizer values in which the numerator and denominator of power localizer cancel each other units so the color-bar has no units
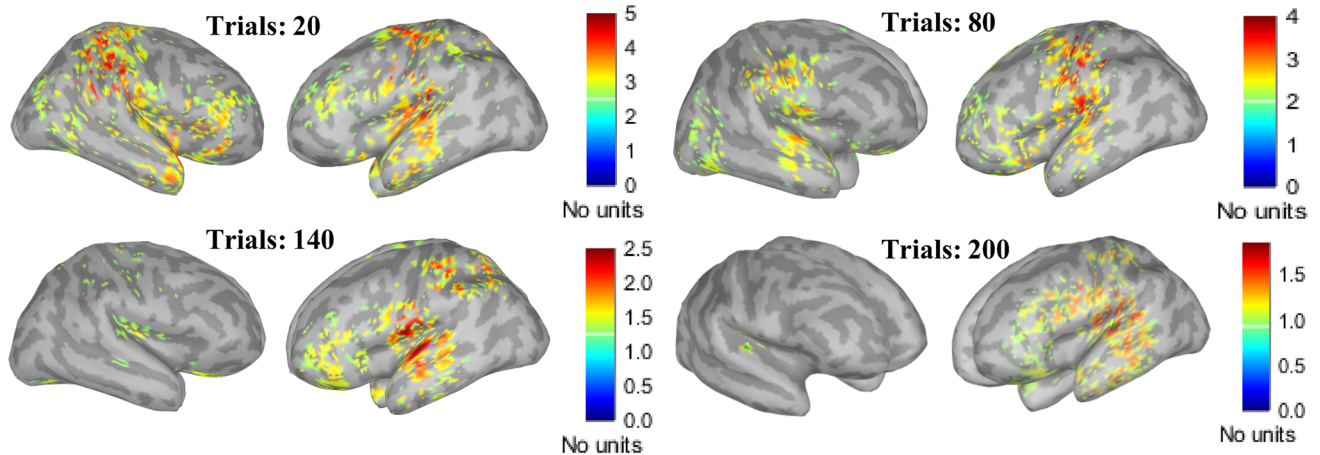

Fig. 10 Investigation of iDMR performance in localizing real AEF data when number of trials varies from 20 to 200 in steps of 60. Green circles existing in right-bottom maps show the primary auditory cortex area. Color-bar values represent the power localizer values in which the numerator and denominator of power localizer cancel each other units so the color-bar has no units

As seen from Fig. 1, based on the FWHM metric, iDMR and eiDMR obtained spatial resolution 7 mm for correlated sources while this value for eMVB was 42 mm and undiagonal iDMR and MVB never reached to their FWHM value. As it is evident at Fig. 3, only iDMR and eiDMR

correctly reconstructed active source time courses in both aspects shape and amplitude.

We ran the second scenario "Evaluation of iDMR performance in comparison to MPZ algorithm" to compare results of iDMR with MPZ method. The latter is known as a suitable technique for dealing with correlated sources. MPZ uses an MVB based recursive procedure for source localization while iDMR performs two step processing, RAP-MUSIC and MVB-based localizer. As a result, iDMR can better handle the correlated sources problem. As illustrated in Fig. 5, iDMR was able to place AEF, SEF, and interference sources in their correct positions whereas MPZ only could do this for SEF one. In contrast to MPZ, iDMR could accurately estimate time courses, Fig. 6.

As a final step, we applied iDMR on real AEF dataset which is available in brainstorm website.[1] Proposed method, iDMR, was able to localize right and left primary auditory cortices, Fig. 9. This scenario results demonstrate that even if over-selection or misplacing or both of them occur by RAP-MUSIC, iDMR can handle it and neglect spurious sources with its second step process, meaning MVB-based localizer. As a result, iDMR is not so sensitive to hyper parameter of RAP-MUSIC, threshold value for algorithm termination.

The proposed method only modifies the data covariance matrix and other elements of which are the same as other MVB-based localizers. Thus, one can use iDMR data covariance matrix for power-based localizers (Moiseev et al. 2011), eigenspace-projection MVB (Sekihara et al. 2001), maximum contrast beamformer (Chen et al. 2006) and many other MVB-based algorithms.

In real AEF dataset scenario, we used the empty room noise for computing **Q** and proper results were obtained. However, since iDMR rebuilds the data covariance matrix using **Q**, it is better to use rest data recorded before the task, for a few minutes. By doing so, we have a data covariance matrix which is similar to original data covariance matrix (5) besides that the sources are decorrelated.

The main idea of iDMR for handling correlated and interference sources is decorrelating source covariance matrix. Hence, one maybe interested to use this feature but replace RAP-MUSIC with other algorithms such as FINES technique which is shown using EEG simulation data that can deals with correlated sources better than RAP-MUSIC (Xu et al. 2004).

Employing RAP-MUSIC, due to using a recursive search throughout the brain, increases computational effort, especially with an increasing number of sources. In a detailed view, implementing iDMR not only requires V beamformer computations (V is the total number of vertices) but also employs $V \times L$ RAP-MUSIC computations to estimate matrix **A** (L denotes the total number of sources found by RAP-MUSIC). As an alternative choice for RAP-MUSIC may source separation algorithms grouped in categories

independent component analysis (ICA) (Hyvärinen et al. 2004) and dependent component analysis (DCA) (Xiang et al. 2015) be useful for determining matrix **A**. Using these algorithms in iDMR can be a topic for future work.

Conclusion

In this work, we investigated the application of iDMR for spatio-temporal reconstruction of neural activities. In situations where the presence of correlated sources or the existence of an interference source can cause an adverse effect particularly in reconstructing the time course of sources, iDMR by removing the cross correlation information from the source covariance matrix outperforms MVB, eMVB, and MPZ algorithms. Through the results acquired from the numerical experiments on both EEG and MEG data and empirical experiment on AEF data it can be understood that iDMR is superior in terms of temporal and spatial resolution, time course reconstruction, and output SNR, with respect to MVB, eMVB, and MPZ.

References

Baillet S, Mosher JC, Leahy RM (2001) Electromagnetic brain mapping. IEEE Signal Process Mag 18(6):14–30

Berg P, Scherg M (1994) A fast method for forward computation of multiple-shell spherical head models. Electroencephalogr Clin Neurophysiol 90(1):58–64

Brookes M, Stevenson C, Barnes G, Hillebrand A, Simpson M, Francis S, Morrisa P (2007) Beamformer reconstruction of correlated sources using a modified source model. Neuroimage 34(4):1454–1465

Brookes MJ, Vrba J, Robinson SE, Stevenson CM, Peters AP, Barnes GR, Hillebrand A, Morris PG (2008) Optimising experimental design for MEG beamformer imaging. Neuroimage 39(4):1788–1802

Chen YS, Cheng CY, Hsieh JC, Chen LF (2006) Maximum contrast beamformer for electromagnetic mapping of brain activity. IEEE Trans Biomed Eng 53(9):1765–1774

Chowdhury RA, Younes Z, Tanguy H, Marcel H, Eliane K, Jean-Marc L, Christophe. G (2015) MEG–EEG information fusion and electromagnetic source imaging: from theory to clinical application in epilepsy. Brain Topogr 18(6):785–812

Dai Y, Zhang W, Dickens DL, He B (2012) Source connectivity analysis from MEG and its application to epilepsy source localization. Brain Topogr 25(2):157–166

Dalal S, Sekihara K, Nagarajan S (2006) Modified beamformers for coherent source region suppression. IEEE Trans Biomed Eng 53(7):1357–1363

Dinh C, Strohmeier D, Luessi M, Güllmar DG, Baumgarten D, Haueisen J, Hamalainen MS (2015) Real-time MEG source localization using regional clustering. Brain Topogr 28(6):771–784

Gorodnitsky J, George, Rao B (1995) Neuromagnetic source imaging with FOCUSS: a recursive weighted minimum norm algorithm. Electroencephalogr Clin Neurophysiol 95(4)231–251

Greenblatt RE, Ossadtchi A, Pflieger ME (2005) Local linear estimators for the bioelectromagnetic inverse problem. IEEE Trans Signal Process 53(9):3403–3412

Haufe S, Arne E (2016) A simulation framework for benchmarking EEG-based brain connectivity estimation methodologies. Brain Topogr. https://doi.org/10.1007/s10548-016-0498-y

Huang M-X, Shih JJ, Lee RR, Harrington DL, Thoma RJ, Weisend MP, Hanlon F, Paulson KM, Li T, Martin K, Miller GA, Canive JM (2004) Commonalities and differences among vectorized beamformers in electromagnetic source imaging. Brain Topogr 16(3):139–158

Hui HB, Pantazis D, Bressler SL, Leahy RM (2010) Identifying true cortical interactions in MEG using the nulling beamformer. Neuroimage 49(4):3161–3174

Hyvärinen A, Karhunen J, Oja E (2004) Independent component analysis, vol 46. Wiley, New York

Jonmohamadi Y, Poudel G, Innes C, Weiss D, Krueger R, Jones R (2014) Comparison of beamformers for EEG source signal reconstruction. Biomed Signal Process Control 14:175–188

Kimura T, Kako M, Kamiyama H, Ishiyama A, Kasai N, Watanabe Y (2007) Inverse solution for time-correlated multiple sources using Beamformer method, vol 1300. International Congress Series, pp 417–420

Mills T, Marc L, Sandra NM, Margot JT, Maher AQ (2012) Techniques for detection and localization of weak hippocampal and medial frontal sources using beamformers in MEG. Brain Topogr 25(3):248–263

Moiseev A, Herdman AT (2013) Multi-core beamformers: derivation, limitations and improvements. Neuroimage 71:135–146

Moiseev A, Gaspar JM, Schneider JA, Herdman AT (2011) Application of multi-source minimum variance beamformers for reconstruction of correlated neural activity. NeuroImage 58(2):481–496

Mosher JC, Leahy RM (1992) Multiple dipole modeling and localization from spatiotemporal MEG data. IEEE Trans Biomed Eng 39(6):541–557

Mosher JC, Leahy RM (1998) Recursive MUSIC: a framework for EEG and MEG source localization. IEEE Trans Biomed Eng 45(11):1342–1354

Mosher JC, Leahy RM (1999) Source localization using recursively applied and projected (RAP) MUSIC. IEEE Trans Signal Process 47(2):332–340

Pascual-Marqui RD (2002) Standardized low resolution brain electromagnetic tomography (sLORETA): technical details. Methods Find Exp Clin Pharmacol 24:5–12

Popescu M, Popescu E, Chan T, Blunt S, Lewine J (2008) Spatial-temporal reconstruction of bilateral auditory steady state responses using MEG beamformers. IEEE Trans Biomed Eng 55(3):1092–1102

Quraan M, Cheyne D (2010) Reconstruction of correlated brain activity with adaptive spatialfilters in MEG. NeuroImage 49(3):2387–2400

Santos EL, Zoltowski MD, Rangaswamy M (2007) Indirect dominant mode rejection: a solution to low sample support beamforming. IEEE Trans Signal Process 55(7):3283–3293

Sekihara K, Nagarajan SS (2008) Adaptive spatial filters for electromagnetic brain imaging. Springer, Berlin

Sekihara K, Nagarajan S, Poeppel D, Marantz A, Miyashita Y (2001) Reconstructing spatio-temporal activities of neural sources using an MEG Vector beamformer technique. IEEE Trans Biomed Eng 48(7):760–771

Sekihara K, Nagarajan S, Poeppel D, Marantz A (2004) Asymptotic SNR of scalar and vector minimum-variance beamformers for neuromagnetic source reconstruction. IEEE Trans Biomed Eng 51(10):1726–1734

Shahbazi F, Ewald A, Nolte G (2015) Self-consistent MUSIC: an approach to the localization of true brain interactions from EEG/MEG data. Neuroimage 112(6):299–309

Tadel F, Baillet S, Mosher JC, Pantazis D, Leahy RM (2011) Brainstorm: a user-friendly application for MEG/EEG analysis. Comput Intell Neurosci. https://doi.org/10.1155/2011/879716

Tikhonov AN, Arsenin VY (1997) Solutions of Ill-posed problems. Wiley, New York, NY

Uutela K, Hamalainen M, Somersalo E (1999) Visualization of magnetoencephalographic data using minimum current estimates. Neuroimage 10(2):173–180

Van Veen B, van Drongelen W, Yuchtman M, Suzuki A (1997) Localization of brain electrical activity via linearly constrained minimum variance spatial filtering. IEEE Trans Biomed Eng 44(9):867–880

Xiang Y, Peng D, Yang Z (2015) Blind source separation: dependent component analysis. Springer, New York

Xu XL, Xu B, He B (2004) An alternative subspace approach to EEG dipole source localization. Phys Med Biol 49:327–343

Yeung N, Bogacz R, Holroyd CB, Cohen JD (2004) Detection of synchronized oscillations in the electroencephalogram: an evaluation of methods. Psychophysiology 41(6)822–832